

Quantum reinforcement learning in the presence of thermal dissipation

María Laura Olivera-Atencio,¹ Lucas Lamata,^{2,3} Manuel Morillo,¹ and Jesús Casado-Pascual^{1,*}

¹*Física Teórica, Universidad de Sevilla, Apartado de Correos 1065, Sevilla 41080, Spain*

²*Departamento de Física Atómica, Molecular y Nuclear, Universidad de Sevilla, 41080 Sevilla, Spain*

³*Instituto Carlos I de Física Teórica y Computacional, 18071 Granada, Spain*

(Dated: August 16, 2022)

A quantum reinforcement learning protocol in the presence of thermal dissipation is introduced and analyzed. Analytical calculations as well as numerical simulations are carried out, obtaining evidence that decoherence and dissipation do not significantly degrade the performance of the quantum reinforcement learning protocol for sufficiently low temperatures, being in some cases even beneficial. Quantum reinforcement learning under realistic experimental conditions of decoherence and dissipation opens an avenue for the realization of quantum agents able to interact with a changing environment, and adapt to it, with plausible many applications inside quantum technologies and machine learning.

I. INTRODUCTION

Quantum machine learning aims at employing quantum technologies for achieving machine learning tasks more efficiently. Given the relevance of machine learning for a plethora of applications in industry and society in general, accelerating these kinds of calculations via quantum devices could seem a highly disruptive possibility.

A diversity of quantum algorithms for machine learning have been proposed, with different kinds of speedups in some cases, including solvers for linear systems of equations [1], quantum principal component analysis [2], quantum support vector machines [3], quantum annealers [4], quantum variational eigensolvers [5], quantum reinforcement learning [6], quantum generative adversarial networks [7], as well as quantum kernels [8]. Initial experimental implementations showing, in some instances, speedups with respect to classical or other kinds of quantum algorithms have been carried out already at the Noisy Intermediate Scale Quantum (NISQ) devices [7–12]. For reviews of the field, we refer to Refs. [6, 13].

In the field of quantum machine learning, there is a parallel classification of quantum algorithms to the classical machine learning field, namely, analogously to supervised, unsupervised, and reinforcement learning algorithms, one can define quantum supervised, quantum unsupervised, and quantum reinforcement learning versions. In this work, we will focus on the latter, namely, quantum reinforcement learning. In this field, several articles have been published, dealing with both theory and experiments [6].

Reinforcement learning algorithms consist on successive interactions between a known agent and an unknown environment alternated with a reward function that improves a specific task performed by such agent [6, 14]. The goal is to learn from the environment. The information extraction from the environment as well as the chan-

nel used to communicate the information to the agent and the action of the agent, are established by the policy. The reward function defines the criterion used to punish or reward certain actions of the agent in order to improve its performance. Each reward reinforces the current strategy while the punishment forces an adaptation of the strategy.

In this paper, we investigate the effect of the presence of dissipation on a quantum reinforcement learning process. For this purpose we consider that the environment corresponds to an unknown quantum system. Its dynamics, besides including a unitary part associated to a given Hamiltonian, also possesses a certain amount of thermal dissipation. One seeks to extract information, or to learn, from that Hamiltonian associated to the unitary part. Specifically, one wants to obtain a nearly optimal knowledge of eigenstates of the Hamiltonian. The agent corresponds to a known and manipulable state that will adapt to the environment dynamics in order to approach the unknown eigenstate. The algorithm employed is based on the one proposed in Ref. [14], where a nondissipative system was studied.

The structure of the remainder of this paper is as follows. In Sec. II, we describe the protocol under consideration with special emphasis on the peculiarities of the dissipative case. In Sec. III, we discuss the numerical implementation of the protocol and illustrate our results with numerical simulations. Finally, in Sec. IV, we present conclusions for the main findings of our work.

II. PROTOCOL DESCRIPTION

In the protocol proposed in Ref. [14], the agent A is considered to be a known manipulable quantum system described by a state vector $|\phi\rangle$. The environment E is modeled as a “black box” that interacts with A for a time τ . The effect of this interaction on A is characterized by a unitary transformation $U \equiv e^{-i\tau H/\hbar}$ applied to the state vector $|\phi\rangle$, where H is an unknown interaction Hamiltonian whose eigenvectors are to be computed. For simplicity, we will henceforth restrict the analysis to the

* jcasado@us.es

case of a single qubit with state basis vectors $\{|0\rangle, |1\rangle\}$ and unknown interaction Hamiltonian

$$H = \frac{\hbar\omega}{2} (|+\rangle\langle+| - |-\rangle\langle-|), \quad (1)$$

where ω is a positive constant with dimensions of frequency and $\{|+\rangle, |-\rangle\}$ are the eigenvectors to be computed.

Suppose now that, in addition to interacting with E, A is also in contact with a thermal bath B at a finite temperature T . We will also assume that the combined action of E and B on A is described by a Lindblad master equation of the form [15]

$$\dot{\rho}_t = -\frac{i}{\hbar}[H, \rho_t] + \sum_{j=\pm} \Gamma_j \left(\tilde{\sigma}_j^\dagger \rho_t \tilde{\sigma}_j - \frac{1}{2} \{ \tilde{\sigma}_j \tilde{\sigma}_j^\dagger, \rho_t \} \right), \quad (2)$$

where ρ_t is the density operator representing the state of A at time t , $\tilde{\sigma}_- = |-\rangle\langle+| = \tilde{\sigma}_+^\dagger$ is a Lindblad operator that induces dissipative decay from the excited state $|+\rangle$ to the ground state $|-\rangle$, and $\Gamma_\pm = \Gamma_0 e^{\pm\hbar\omega/(2k_B T)} \text{csch}[\hbar\omega/(2k_B T)]/2$, with Γ_0 being the decay rate from the excited state to the ground state at zero temperature. The frequency ω in Eq. (1) must be redefined to include the frequency shift caused by the presence of the thermal bath. The first term on the right hand side in Eq. (2) describes the coherent evolution of the system, while the second term gives rise to dissipation.

By solving Eq. (2), the density operator at an arbitrary time τ can be expressed in terms of the initial density operator ρ_0 in the form

$$\rho_\tau = \mathcal{E}(\rho_0) \equiv \sum_{j=0}^3 U E_j \rho_0 E_j^\dagger U^\dagger, \quad (3)$$

where $\{E_0, E_1, E_2, E_3\}$ are the Kraus operators for the generalized amplitude damping channel [16]. The explicit expressions for these operators are [16]

$$E_0 = \sqrt{p_+} \left(|+\rangle\langle+| + \sqrt{1-\gamma} |-\rangle\langle-| \right), \quad (4)$$

$$E_1 = \sqrt{p_+ \gamma} \tilde{\sigma}_+, \quad (5)$$

$$E_2 = \sqrt{1-p_+} \left(\sqrt{1-\gamma} |+\rangle\langle+| + |-\rangle\langle-| \right), \quad (6)$$

$$E_3 = \sqrt{(1-p_+)\gamma} \tilde{\sigma}_-, \quad (7)$$

where $p_+ = e^{-\hbar\omega/(2k_B T)} \text{sech}[\hbar\omega/(2k_B T)]/2$ is the thermal equilibrium probability of the excited state and $\gamma = 1 - e^{-\Gamma\tau}$, with $\Gamma = \Gamma_+ + \Gamma_- = \Gamma_0 \coth[\hbar\omega/(2k_B T)]$. Note that in the absence of dissipation, i.e., for $\Gamma_0 = 0$, the parameter γ vanishes and, therefore, $E_0 = \sqrt{p_+} I$, $E_2 = \sqrt{1-p_+} I$, and $E_1 = E_3 = 0$, with I being the identity operator. Thus, Eq. (3) reduces to $\rho_\tau = U \rho_0 U^\dagger$, which is the case considered in Ref. [14] with $\rho_0 = |\phi\rangle\langle\phi|$.

Bearing in mind the above results, the protocol proposed in Ref. [14] can be adapted to the dissipative case as detailed below. The procedure involves very many iterations, so that, the state of A in the k th iteration is

denoted as $|\phi^{(k)}\rangle$, with $k \in \mathbb{N}$. We assume that, in the first iteration, A is prepared in one of the basis states, specifically in the state $|\phi^{(1)}\rangle = |0\rangle$. The states $|0\rangle$ and $|\phi^{(k)}\rangle$ are related by

$$|\phi^{(k)}\rangle = D^{(k)} |0\rangle. \quad (8)$$

where $D^{(k)}$ is a unitary operator constructed inductively, starting with $D^{(1)} = I$, and building $D^{(k+1)}$ out of $D^{(k)}$ as follows:

(i) From the initial density operator $\rho_0^{(k)} = |\phi^{(k)}\rangle\langle\phi^{(k)}|$, we let the system evolve according to the Lindblad equation in Eq. (2) for a time τ . Call $\rho_\tau^{(k)} = \mathcal{E}(\rho_0^{(k)})$ the density at the end of that evolution obtained by Eq. (3).

(ii) We extract information from $\rho_\tau^{(k)}$ by measuring the observable $M^{(k)} = D^{(k)} |1\rangle\langle 1| D^{(k)\dagger}$. In order to always measure the same observable $M^{(1)} = |1\rangle\langle 1|$ for all iterations, first, we apply the unitary transformation $D^{(k)\dagger} \rho_\tau^{(k)} D^{(k)}$ and, then, we measure $M^{(1)}$. After the measurement process, the state of A is $|m^{(k)}\rangle$, with $m^{(k)}$ being the outcome of the measurement, which can be 0 or 1 with probabilities

$$P_0^{(k)} = \langle 0 | D^{(k)\dagger} \rho_\tau^{(k)} D^{(k)} | 0 \rangle \quad (9)$$

and $P_1^{(k)} = 1 - P_0^{(k)}$, respectively. Once the measurement has been completed, the state $|\phi^{(k)}\rangle$ can be reconstructed from $|m^{(k)}\rangle$ by the unitary transformation $D^{(k)} [(1 - m^{(k)})I + m^{(k)}\sigma_x] |m^{(k)}\rangle$, with $\sigma_x = |0\rangle\langle 1| + |1\rangle\langle 0|$.

(iii) If the outcome of the measurement is $m^{(k)} = 1$, we generate three pseudo-random angles, $\alpha_x^{(k)}$, $\alpha_y^{(k)}$, and $\alpha_z^{(k)}$, uniformly distributed in the interval $[-w^{(k)}\pi, w^{(k)}\pi]$. The width of the interval is controlled by the exploration parameter $w^{(k)}$, which is computed inductively, starting with $w^{(1)} = 1$ (maximum width), and building $w^{(k+1)}$ out of $w^{(k)}$ using the rule

$$w^{(k+1)} = \max \left\{ 1, \left[(1 - m^{(k)})r + m^{(k)}p \right] w^{(k)} \right\}, \quad (10)$$

with $r < 1$ and $p > 1$ being the reward and the punishment rates [14], respectively. Then, we use these three angles to implement the pseudo-random rotation

$$R^{(k)} = e^{-i\alpha_y^{(k)}\sigma_y/2} e^{-i\alpha_z^{(k)}\sigma_z/2} e^{-i\alpha_x^{(k)}\sigma_x/2}, \quad (11)$$

where the operators $\sigma_x^{(k)}$, $\sigma_y^{(k)}$, and $\sigma_z^{(k)}$ are related to the Pauli operators σ_x , $\sigma_y = i(|1\rangle\langle 0| - |0\rangle\langle 1|)$, and $\sigma_z = |0\rangle\langle 0| - |1\rangle\langle 1|$ by the unitary transformation $\sigma_\alpha^{(k)} = D^{(k)} \sigma_\alpha D^{(k)\dagger}$, with $\alpha = x, y$, and z .

(iv) Finally, we construct $D^{(k+1)}$ from $D^{(k)}$ as

$$D^{(k+1)} = \left[(1 - m^{(k)})I + m^{(k)}R^{(k)} \right] D^{(k)}. \quad (12)$$

Since, according to Eq. (11), $R^{(k)}$ is related to the random rotation

$$\check{R}^{(k)} = e^{-i\alpha_y^{(k)}\sigma_y/2} e^{-i\alpha_z^{(k)}\sigma_z/2} e^{-i\alpha_x^{(k)}\sigma_x/2} \quad (13)$$

by the unitary transformation $R^{(k)} = D^{(k)}\check{R}^{(k)}D^{(k)\dagger}$, Eq. (12) can also be expressed in the form

$$D^{(k+1)} = D^{(k)} \left[(1 - m^{(k)})I + m^{(k)}\check{R}^{(k)} \right]. \quad (14)$$

The recursive relations in Eqs. (12) and (14) can easily be solved to yield

$$D^{(k+1)} = \prod_{j=k}^1 \left[(1 - m^{(j)})I + m^{(j)}R^{(j)} \right] \quad (15)$$

and

$$D^{(k+1)} = \prod_{j=1}^k \left[(1 - m^{(j)})I + m^{(j)}\check{R}^{(j)} \right], \quad (16)$$

respectively, where we use the ordered product notation $\prod_{j=k}^1 A_j = A_k A_{k-1} \cdots A_1$ and $\prod_{j=1}^k A_j = A_1 A_2 \cdots A_k$. Note that the randomness of the unitary operator $D^{(k+1)}$ comes from two sources. The first is the intrinsic randomness of the measurement outcomes $m^{(j)}$ for $1 \leq j \leq k$. The second source of randomness results from the dependence of the rotations $R^{(j)}$ and $\check{R}^{(j)}$ on the pseudo-random angles $\alpha_x^{(j)}$, $\alpha_y^{(j)}$, and $\alpha_z^{(j)}$.

III. NUMERICAL RESULTS

We have carried out numerical simulations implementing the protocol presented in the previous section for a Hamiltonian of the form

$$H = \frac{\hbar\omega}{2} \sigma_x, \quad (17)$$

which corresponds to taking $|\pm\rangle = (|0\rangle \pm |1\rangle)/\sqrt{2}$ in Eq. (1). To deal with dimensionless quantities, we have introduced the dimensionless parameters $\tilde{\tau} = \omega\tau$, $\tilde{\Gamma}_0 = \Gamma_0/\omega$, and $\tilde{T} = k_B T/(\hbar\omega)$. To simulate numerically the measurement process appearing in item (ii) of Sec. II, we first calculate the probability $P_0^{(k)}$ of obtaining $m^{(k)} = 0$ using Eq. (9). Then, we draw a pseudo-random number $\xi^{(k)}$ uniformly distributed in the interval $[0, 1]$. If $\xi^{(k)} \leq P_0^{(k)}$, the outcome of the measurement is $m^{(k)} = 0$, whereas if $\xi^{(k)} > P_0^{(k)}$ the result will be $m^{(k)} = 1$.

In order to assess the accuracy of the protocol, we have calculated the fidelity between the state $|\phi^{(k)}\rangle$ and the closest eigenvector of H as a function of the iteration number k . Since it is not known *a priori* whether this eigenvector is $|+\rangle$ or $|-\rangle$, we have considered the greater of the two values, i.e.,

$$f^{(k)} = \max \left(|\langle +|\phi^{(k)}\rangle|, |\langle -|\phi^{(k)}\rangle| \right). \quad (18)$$

The closer the value of $f^{(k)}$ is to 1 as k increases, the more accurate the computation of the corresponding eigenvector will be. In addition, at each iteration, the convergence

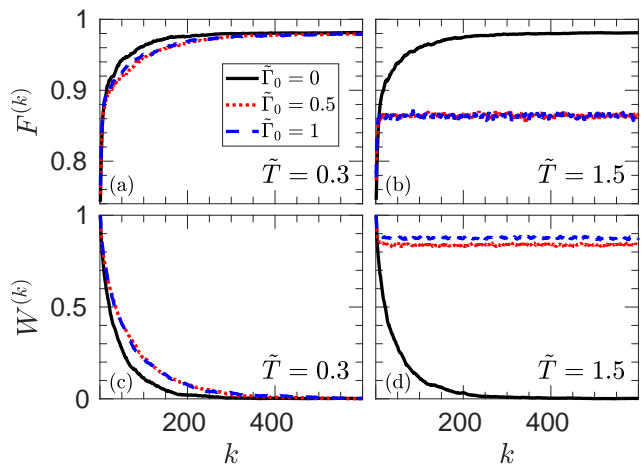


FIG. 1. Dependence of the mean fidelity $F^{(k)}$ [(a) and (b)] and the mean exploration parameter $W^{(k)}$ [(c) and (d)] on the iteration number k . Black solid lines depict the nondissipative case $\tilde{\Gamma}_0 = 0$. The dissipative cases are indicated with red dotted lines ($\tilde{\Gamma}_0 = 0.5$) and blue dashed lines ($\tilde{\Gamma}_0 = 1$). The dimensionless temperature is $\tilde{T} = 0.3$ in (a) and (c) and $\tilde{T} = 1.5$ in (b) and (d). The remaining parameter values are $\tilde{\tau} = 1$, $N = 1000$, $r = 0.9$, and $p = 2/r$.

of the protocol has been quantified by the exploration parameter $w^{(k)}$ defined in item (iii) of Sec. II. The protocol is considered to converge if $w^{(k)}$ approaches zero as the iteration number k increases. Moreover, the faster it approaches zero, the faster the convergence of the protocol.

In the numerical simulations presented here, we have repeated the protocol a large number N of realizations, all of them starting from the same initial state $|\phi^{(1)}\rangle = |0\rangle$ of A . Then, for each iteration number k , the mean fidelity

$$F^{(k)} = \frac{1}{N} \sum_{j=1}^N f_j^{(k)} \quad (19)$$

and the mean exploration parameter

$$W^{(k)} = \frac{1}{N} \sum_{j=1}^N w_j^{(k)} \quad (20)$$

are obtained by averaging over the N realizations, where the subscript j refers to the j th realization of the protocol. The number of realizations considered in this paper is $N = 1000$.

In Fig. 1 we have plotted the mean fidelity $F^{(k)}$ [(a) and (b)] and the mean exploration parameter $W^{(k)}$ [(c) and (d)] versus the iteration number k for the parameter values indicated in the figure caption. With different types of lines, we have depicted different values of the dimensionless decay rate at zero temperature $\tilde{\Gamma}_0$. The figure illustrates the role played by the temperature in the accuracy and convergence of the protocol. For dimensionless temperature $\tilde{T} = 0.3$ [(a) and (c)], the differences between the nondissipative case $\tilde{\Gamma}_0 = 0$ (solid black

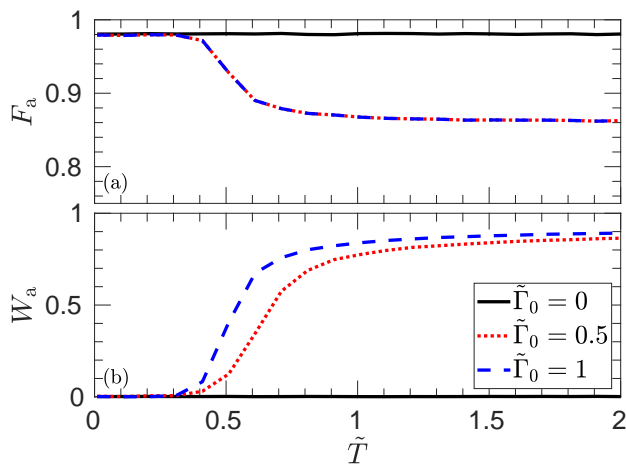


FIG. 2. Dependence of the asymptotic values in the large iteration limit of the mean fidelity, F_a , and the mean exploration parameter, W_a , on the dimensionless temperature \tilde{T} for different values of $\tilde{\Gamma}_0$. Black solid lines depict the nondissipative case $\tilde{\Gamma}_0 = 0$, while the dissipative cases are indicated with red dotted lines ($\tilde{\Gamma}_0 = 0.5$) and blue dashed lines ($\tilde{\Gamma}_0 = 1$). The remaining parameter values are $\tilde{\tau} = 1$, $N = 1000$, $r = 0.9$, and $p = 2/r$.

line), and the dissipative cases $\tilde{\Gamma}_0 = 0.5$ (dotted red line) and $\tilde{\Gamma}_0 = 1$ (blue dashed line) are not very significant. In the three cases, the asymptotic values of $F^{(k)}$ in the large iteration limit are very similar and quite close to 1 [see Fig. 1(a)], and $W^{(k)}$ converges to zero rather quickly [see Fig. 1(c)]. Therefore, contrary to what might be expected, temperatures much lower than $\hbar\omega/k_B$ are not required for the protocol to work. Nonetheless, for sufficiently high dimensionless temperatures, such as $\tilde{T} = 1.5$, the protocol fails in the dissipative cases, as shown in Figs. 1(b) and (d). On the one hand, the asymptotic values of $F^{(k)}$ in the large iteration limit are substantially less than in the absence of dissipation [see Fig. 1(b)]. On the other hand, $W^{(k)}$ does not approach zero as k increases [see Fig. 1(d)] and, therefore, the protocol does not converge.

In order to determine the range of temperatures in which the protocol works, in Fig. 2 we have plotted the asymptotic values in the large iteration limit of the mean fidelity, F_a , and the mean exploration parameter, W_a , as a function of the dimensionless temperature \tilde{T} . As can be seen, there is hardly any difference between the dissipative and nondissipative cases up to $\tilde{T} \approx 0.4$. Above that temperature, the F_a values in the dissipative cases $\tilde{\Gamma}_0 = 0.5$ (red dotted line) and $\tilde{\Gamma}_0 = 1$ (blue dashed line) decrease abruptly and become substantially less than in the nondissipative case [see Fig. 2(a)]. Furthermore, there is a rapid increase in W_a to nonzero values [see Fig. 2(b)], which indicates that the protocol stops converging.

To better understand the behavior observed in Fig. 2, it is worth remembering that, in the nondissipative case, the design of the protocol is based on the fact that the

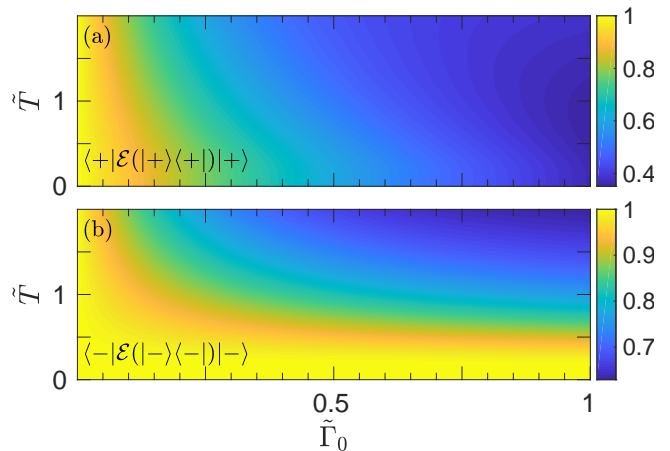


FIG. 3. Dependence of the fidelities $\langle +|\mathcal{E}(|+\rangle\langle +|)|+\rangle$ in Eq. (21) and $\langle -|\mathcal{E}(|-\rangle\langle -|)|-\rangle$ in Eq. (22) on $\tilde{\Gamma}_0$ and \tilde{T} for $\tilde{\tau} = 1$, $N = 1000$, $r = 0.9$, and $p = 2/r$.

states $|+\rangle\langle +|$ and $|-\rangle\langle -|$ are fixed points of the quantum gate \mathcal{E} , i.e., $\mathcal{E}(|\pm\rangle\langle \pm|) = |\pm\rangle\langle \pm|$. However, in the presence of dissipation, $|+\rangle\langle +|$ and $|-\rangle\langle -|$ are no longer exact fixed points of \mathcal{E} , since the fidelities between the state $|+\rangle\langle +|$ and $\mathcal{E}(|+\rangle\langle +|)$, $\langle +|\mathcal{E}(|+\rangle\langle +|)|+\rangle$, and between the state $|-\rangle\langle -|$ and $\mathcal{E}(|-\rangle\langle -|)$, $\langle -|\mathcal{E}(|-\rangle\langle -|)|-\rangle$, are in general less than 1. Specifically, from Eq. (3), it can be shown that

$$\langle +|\mathcal{E}(|+\rangle\langle +|)|+\rangle = 1 - (1 - p_+) \gamma \quad (21)$$

$$\langle -|\mathcal{E}(|-\rangle\langle -|)|-\rangle = 1 - p_+ \gamma, \quad (22)$$

which are clearly less than 1 if $\tilde{\Gamma}_0 \neq 0$ (dissipative case). Despite this, there may be parameter values for which the fidelities $\langle +|\mathcal{E}(|+\rangle\langle +|)|+\rangle$ and/or $\langle -|\mathcal{E}(|-\rangle\langle -|)|-\rangle$ are quite close to 1. In that case, the corresponding states $|+\rangle\langle +|$ and/or $|-\rangle\langle -|$ would behave as approximate fixed points and the protocol would still be applicable. Figure 3 shows the dependence of the fidelities $\langle +|\mathcal{E}(|+\rangle\langle +|)|+\rangle$ and $\langle -|\mathcal{E}(|-\rangle\langle -|)|-\rangle$, obtained using Eqs. (21) and (22), on $\tilde{\Gamma}_0$ and \tilde{T} . As can be seen, there are regions where these fidelities are quite close to 1. In particular, Fig. 3(b) shows that $\langle -|\mathcal{E}(|-\rangle\langle -|)|-\rangle$ is quite close to 1 up to $\tilde{T} \approx 0.4$, which is the approximate value beyond which the protocol starts to fail in Fig. 2.

From Figs. 1 and 2, it may be concluded that the effect of dissipation is not very relevant for sufficiently low dimensionless temperatures. However, a more exhaustive analysis of the results reveals that it plays an important role in the protocol. Figure 4 depicts separately the mean fidelity $F_-^{(k)}$ between the state $|\phi^{(k)}\rangle$ and the ground state $|-\rangle$ [(a) and (b)] and the mean fidelity $F_+^{(k)}$ between the state $|\phi^{(k)}\rangle$ and the excited state $|+\rangle$ [(c) and (d)], defined as

$$F_{\mp}^{(k)} = \frac{1}{N} \sum_{j=1}^N |\langle \mp | \phi^{(k)} \rangle|. \quad (23)$$

While, for $\tilde{T} = 0.3$, the differences between the dissipa-

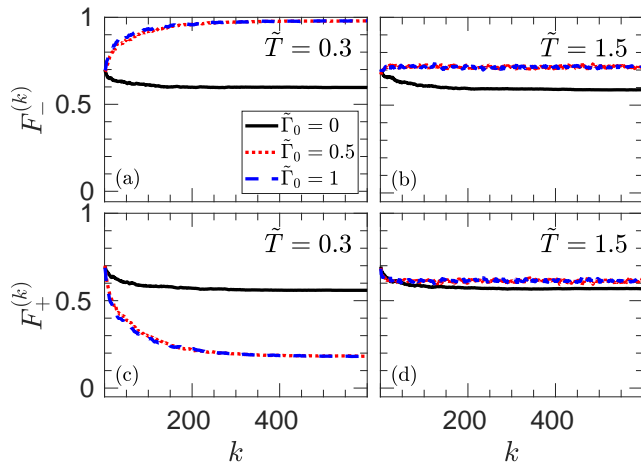


FIG. 4. Dependence of the state-specific mean fidelities $F_-^{(k)}$ [(a) and (c)] and $F_+^{(k)}$ [(b) and (d)] on the iteration number k . Black solid lines depict the nondissipative case $\tilde{\Gamma}_0 = 0$. The dissipative cases are indicated with red dotted lines ($\tilde{\Gamma}_0 = 0.5$) and blue dashed lines ($\tilde{\Gamma}_0 = 1$). The dimensionless temperature is $\tilde{T} = 0.3$ in (a) and (c) and $\tilde{T} = 1.5$ in (b) and (d). The remaining parameter values are $\tilde{\tau} = 1$, $N = 1000$, $r = 0.9$, and $p = 2/r$.

tive and nondissipative cases are not too significant when comparing the mean fidelity $F^{(k)}$ [see Fig. 1(a)], they become rather noticeable when comparing the state-specific mean fidelities $F_-^{(k)}$ and $F_+^{(k)}$ [see Figs. 4(a) and (c)]. In the nondissipative case, $F_-^{(k)}$ and $F_+^{(k)}$ are almost indistinguishable [black solid lines in Figs. 4(a) and (c)], as is to be expected from the fact that $|+\rangle\langle+|$ and $|-\rangle\langle-|$ are equivalent fixed points \mathcal{E} in the absence of dissipation. By contrast, the presence of dissipation substantially affects the state-specific fidelities, increasing $F_-^{(k)}$ and decreasing $F_+^{(k)}$ [red dotted lines and blue dashed lines in Figs. 4(a) and (c)]. This is because, for $\tilde{T} = 0.3$, $\tilde{\Gamma}_0 = 0.5$ and $\tilde{\Gamma}_0 = 1$, $|-\rangle\langle-|$ is an approximate fixed point of \mathcal{E} but $|+\rangle\langle+|$ is not [see Fig. 3]. As the temperature increases, this difference becomes less appreciable, as can be seen in Figs. 4(b) and (d).

One important aspect, not considered so far, is the dependence of the protocol results on the evolution time τ . As mentioned in Sec. II, in the absence of dissipation, i.e., for $\Gamma_0 = 0$, the action of \mathbf{E} on \mathbf{A} is represented by the quantum channel $\mathcal{E}(\rho_0) = e^{-i\tau H/\hbar}\rho_0 e^{i\tau H/\hbar}$. For the case of the Hamiltonian H in Eq. (17), this quantum channel has the explicit form

$$\begin{aligned} \mathcal{E}(\rho_0) = & \frac{1}{2}(\rho_0 + \sigma_x \rho_0 \sigma_x) \\ & + \frac{\cos(\tilde{\tau})}{2}(\rho_0 - \sigma_x \rho_0 \sigma_x) + \frac{i \sin(\tilde{\tau})}{2}[\rho_0, \sigma_x], \end{aligned} \quad (24)$$

which is a periodic function of the dimensionless evolution time $\tilde{\tau}$ with period 2π . This periodicity is clearly visible in Fig. 5(a), where the dependence of F_a on $\tilde{\tau}$ in the nondissipative case is depicted with a solid line. However, the periodicity is not evident in the behavior of

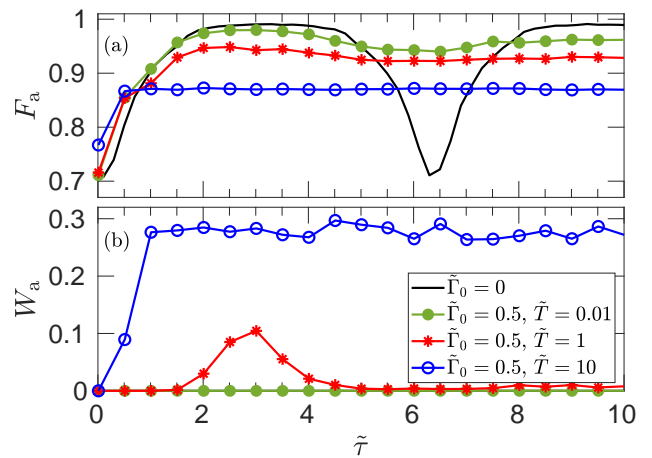


FIG. 5. Dependence of the asymptotic values in the large iteration limit of the mean fidelity, F_a , and the mean exploration parameter, W_a , on the dimensionless evolution time $\tilde{\tau}$ for different values of $\tilde{\Gamma}_0$ and \tilde{T} . Black solid lines depict the nondissipative case $\tilde{\Gamma}_0 = 0$. In (b) the black solid line is indistinguishable from the abscissa-axis. The dissipative cases are indicated with green filled circles ($\tilde{\Gamma}_0 = 0.5$ and $\tilde{T} = 0.01$), red stars ($\tilde{\Gamma}_0 = 0.5$ and $\tilde{T} = 1$), and blue open circles ($\tilde{\Gamma}_0 = 0.5$ and $\tilde{T} = 10$). The remaining parameter values are $N = 1000$, $r = 0.9$, and $p = 2/r$.

W_a , which always remains close to 0 and indistinguishable from the abscissa-axis, as shown in Fig. 5(b). Of particular interest is the case in which $\tilde{\tau}$ is an integer multiple of 2π . In this case, it follows from Eq. (24) that \mathbf{E} does not modify the state of \mathbf{A} and, therefore, no learning is possible. Thus, the mean fidelity $F^{(k)}$ is independent of the iteration number k and, consequently, $F_a = F^{(1)} = 1/\sqrt{2} \approx 0.71$, as can be observed in Fig. 5(a) (black solid line).

In the presence of dissipation, i.e., for $\Gamma_0 \neq 0$, the quantum channel $\mathcal{E}(\rho_0)$ in Eq. (3) ceases to be periodic in $\tilde{\tau}$ due to the exponential dependence of the parameter γ on the evolution time τ (see Sec. II). As a consequence, the oscillations observed in Fig. 5(a) for the nondissipative case (black solid line) are notably attenuated and, beyond a certain value of $\tilde{\tau}$, F_a becomes almost independent of $\tilde{\tau}$ [see green filled circles, red stars, and blue open circles in Fig. 5(a)]. The effect of temperature on the behavior of F_a is quite revealing. The long $\tilde{\tau}$ values of F_a for the dissipative case decrease as the temperature increases, as expected. Nonetheless, the F_a values are substantially larger than those for the nondissipative case for $\tilde{\tau}$ values around the integer multiples of 2π . Therefore, under these circumstances, dissipation plays a positive role in the protocol fidelity. Note that for not too high temperatures, the convergence of the protocol gauged by W_a is still guaranteed around the above mentioned $\tilde{\tau}$ values [see green filled circles and red stars in Fig. 5(b)].

IV. CONCLUSIONS

In this work, we have implemented a protocol for reinforcement learning in a dissipative situation. This is accomplished by introducing a Lindblad dynamics for the density operator for a two state system in contact with a thermal bath. First, we have presented a detailed theoretical analysis of the protocol and defined the relevant quantities that will characterize it. Next, a numerical analysis of the protocol is carried out to exemplify its usefulness as fidelities near unity are obtained.

The main conclusions of this work are:

(i) For sufficiently low temperatures, dissipation does not necessarily have a negative effect on the accuracy of the protocol gauged by the mean fidelity $F^{(k)}$. In fact, our analysis shows that there are ranges of parameter values for which the dissipative protocol performs better than the nondissipative one, as can be seen in Fig. 5. These results might be of interest for the experimental implementation of this type protocols, since sometimes the presence of dissipation is unavoidable in an actual experiment.

(ii) Dissipation is particularly relevant when evaluating the state-specific mean fidelities $F_-^{(k)}$ and $F_+^{(k)}$. The influence of dissipation on these fidelities depends dramatically on which state-specific is considered. While in the nondissipative case $F_-^{(k)}$ and $F_+^{(k)}$ are almost indistinguishable, in the dissipative case they can be quite different. Specifically, for sufficiently low temperatures, the mean fidelity with respect to the ground state, $F_-^{(k)}$, is much higher than the one obtained in the absence of dissipation, whereas the mean fidelity with respect to the excited state, $F_+^{(k)}$, is much lower. Therefore, if in an actual experiment one were interested in specifically computing the ground state, the presence of dissipation might be useful.

ACKNOWLEDGEMENTS

We acknowledge funding by the Junta de Andalucía (P20-00617 and US-1380840) and by the Spanish Ministry of Science, Innovation, and Universities under grant Nos. PID2019-104002GB-C21 and PID2019-104002GB-C22.

-
- [1] A. W. Harrow, A. Hassidim, and S. Lloyd, *Phys. Rev. Lett.* **103**, 150502 (2009).
 - [2] S. Lloyd, M. Mohseni, and P. Rebentrost, *Nature Phys.* **10**, 631 (2014).
 - [3] P. Rebentrost, M. Mohseni, and S. Lloyd, *Phys. Rev. Lett.* **113**, 130503 (2014).
 - [4] R. K. Nath, H. Thapliyal, and T. S. Humble, *SN Comp. Sci.* **2**, 365 (2021).
 - [5] J. R. McClean, J. Romero, R. Babbush, and A. Aspuru-Guzik, *New J. Phys.* **18**, 023023 (2016).
 - [6] L. Lamata, *Mach. Learn. Sci. Technol.* **1**, 033002 (2020).
 - [7] L. Hu, S.-H. Wu, W. Cai, Y. Ma, X. Mu, Y. Xu, H. Wang, Y. Song, D.-L. Deng, C.-L. Zou, and L. Sun, *Sci. Adv.* **5**, eaav2761 (2019).
 - [8] V. Havlíček, A. D. Córcoles, K. Temme, A. W. Harrow, A. Kandala, J. M. Chow, and J. M. Gambetta, *Nature* **567**, 209 (2019).
 - [9] S. Yu, F. Albarrán-Arriagada, J. C. Retamal, Y.-T. Wang, W. Liu, Z.-J. Ke, Y. Meng, Z.-P. Li, J.-S. Tang, E. Solano, L. Lamata, C.-F. Li, and G.-C. Guo, *Adv. Quantum Technol.* **2**, 1800074 (2019).
 - [10] V. Saggio, B. E. Asenbeck, A. Hamann, T. Strömberg, P. Schiansky, V. Dunjko, N. Friis, N. C. Harris, M. Hochberg, D. Englund, S. Wölk, H. J. Briegel, and P. Walther, *Nature* **591**, 229 (2021).
 - [11] M. Spagnolo, J. Morris, S. Piacentini, M. Antesberger, F. Massa, A. Crespi, F. Ceccarelli, R. Osellame, and P. Walther, *Nature Phot.* **16**, 318 (2022).
 - [12] H.-Y. Huang, M. Broughton, J. Cotler, S. Chen, J. Li, M. Mohseni, H. Neven, R. Babbush, R. Kueng, J. Preskill, and J. R. McClean, *Science* **376**, 1182 (2022).
 - [13] J. Biamonte, P. Wittek, N. Pancotti, P. Rebentrost, N. Wiebe, and S. Lloyd, *Nature* **549**, 195 (2017).
 - [14] F. Albarrán-Arriagada, J. C. Retamal, E. Solano, and L. Lamata, *Mach. Learn.: Sci. Technol.* **1**, 015002 (2020).
 - [15] H.-P. Breuer and F. Petruccione, *Theory of Open Quantum Systems* (Oxford University Press, Oxford, 2003).
 - [16] M. A. Nielsen and I. L. Chuang, *Quantum Computing and Quantum Information* (Cambridge University Press, Cambridge, 2000).